HHS Public Access

Author manuscript

Sci Transl Med. Author manuscript; available in PMC 2018 August 07.

Published in final edited form as:

Sci Transl Med. 2018 February 07; 10(427): . doi:10.1126/scitranslmed.aan5372.

Targeting mitochondrial responses to intra-articular fracture to prevent posttraumatic osteoarthritis

Mitchell C. Coleman[1,*], **Jessica E. Goetz**[1], **Marc J. Brouillette**[1], **Dongrim Seol**[1], **Michael C. Willey**[1], **Emily B. Petersen**[1], **Hope D. Anderson**[2], **Nathan R. Hendrickson**[1], **Jocelyn T. Compton**[1], **Behnoush Khorsand**[1], **Angie S. Morris**[1], **Aliasger K. Salem**[1], **Douglas C. Fredericks**[1], **Todd O. McKinley**[3], and **James A. Martin**[1]

[1]University of Iowa, Iowa City, IA 52242.

[2]Wellesley College, Boston, MA 02481.

[3]Indiana University Health Methodist Hospital Orthopaedic Trauma Service, Indianapolis, IN 46202.

Abstract

We tested whether inhibiting mechanically-responsive articular chondrocyte mitochondria after severe traumatic injury and preventing oxidative damage represent a viable paradigm for posttraumatic osteoarthritis (PTOA) prevention. We used a porcine hock intra-articular fracture (IAF) model well suited to human-like surgical techniques and with excellent anatomic similarities to human ankles. After IAF, amobarbital or *N*-acetylcysteine (NAC) was injected to inhibit chondrocyte electron transport or downstream oxidative stress, respectively. Effects were confirmed via spectrophotometric enzyme assays or glutathione/glutathione disulfide assays and immunohistochemical measures of oxidative stress. Amobarbital or NAC delivered after IAF provided substantial protection against PTOA at 6 months, including maintenance of proteoglycan content, decreased histological disease scores, and normalized chondrocyte metabolic function. These data support the therapeutic potential of targeting chondrocyte metabolism after injury and suggest a strong role for mitochondria in mediating PTOA.

[*]Corresponding author: mitchell-coleman@uiowa.edu.

Author contributions: M.C.C. contributed to the design, execution, and interpretation of all experiments and wrote the manuscript. J.E.G. contributed to the design, execution, and interpretation of all porcine experiments and histological analysis and assisted in writing the manuscript. M.J.B. contributed to the design, execution, and interpretation of all mitochondrial and in vitro experiments and assisted in writing the manuscript. DS contributed to the design, execution, and interpretation of all porcine experiments using hydrogel injections and assisted in writing the manuscript. M.C.W. contributed to the design, execution, and interpretation of all porcine experiments, performed the porcine surgeries and assisted in writing the manuscript. E.B.P. contributed to the design, execution, and interpretation of all animal experiments, assisted in animal surgeries and assisted in writing the manuscript. B.K., A.S.M., and A.K.S. contributed to the design, execution, and interpretation of all PLGA experiments and assisted in writing the manuscript. D.C.F. contributed to the design, execution, and interpretation of all animal experiments, performed the animal surgeries and assisted in writing the manuscript. T.O.M. contributed to the design, execution, and interpretation of all porcine experiments, performed the porcine surgeries and assisted in writing the manuscript. J.A.M. supervised the design, execution, and interpretation of all porcine experiments and assisted in writing the manuscript..

Competing interests: Authors M.C.C., M.J.B., T.O.M., and J.A.M. have filed a patent via the University of Iowa related to the treatment hydrogels utilized in this study, WO2017031214A1, PCT/US2016/047360, Preventative therapy for post-traumatic osteoarthritis. A.K.S. serves on the advisory board of Cartilagen LLC, and JAMJ.A.M. serves as scientific advisor to Cartilagen LLC, which licenses the patent WO2017031214A1. All other authors declare that they have no competing interests.

Introduction

Posttraumatic osteoarthritis (PTOA), the progressive destruction of articular cartilage in synovial joints after injury, afflicts more than 5.6 million Americans with total costs exceeding $3 billion annually as of 2006 (1). This disease affects a disproportionately large number of active, young people and carries quality of life issues comparable to congestive heart failure or kidney disease (2, 3). Despite considerable improvements in posttraumatic surgical care, any intra-articular fracture (IAF) in a load-bearing joint still carries the same risk of PTOA as it would have forty years ago, with more severe fractures ultimately progressing to PTOA almost uniformly (4–8). In the ankle where osteoarthritis without injury is rare, rapid progression to PTOA occurs by two years in 35% of patients and by 4 years in 55% of patients, often at relatively young ages. Given that there remain no treatments beyond fracture fixation available before end-stage joint replacement or fusion, there is an immediate unmet need for strategies to prevent or forestall PTOA that can be applied after IAF and before or alongside standard open reduction and internal fixation (ORIF) procedures.

The standard course of patient care after an IAF describes an early treatment window for potential adjunctive treatments spanning patients' initial emergency room visits through surgical fixation, with opportunities for intervention dwindling rapidly thereafter. Although the value of this early window has been recognized and descriptions of early intracellular pathology have noted mitochondrial involvement (9–11), the specific mechanisms linking acute injury, mitochondrial response, and chronic disease are only partially understood. What is known is that immediately after injurious cartilage impact, articular chondrocytes within and around impact sites respond with a burst of mitochondrial activity and produce damaging amounts of reactive oxygen species (ROS) (12–16). This is accompanied by mitochondrial swelling and changes in polarization, hallmark features of disrupted mitochondrial physiology (11, 17–19). Recently, a somewhat similar pathway that relies on complicated dysfunction of the electron transport chain (ETC) has been identified in ischemia/reperfusion (IR) injuries common in cardiovascular settings (20, 21). Succinate accumulation during ischemia results in catastrophic reverse electron transport upon return of blood and oxygen to the tissue (reperfusion). Thus, the sequential combination of lack of oxygen, succinate accumulation, and return of oxygen drives oxidative injury through reverse electron transport.

We hypothesize that the exposure of the articular surface to blood after IAF subjects the chondrocytes to a bolus of metabolites and oxygen that may be injurious to articular cartilage in a manner somewhat similar to IR injuries but with important differences related to the physiological milieu of the synovial joint. Here, we propose that the influx of blood and oxygen onto normally hypoxic cartilage combined with the mechanical injury associated with fracture results in an exaggerated and catastrophic electron transport response. Previous results have demonstrated that cumulative oxidative damage from mitochondrial dysfunction and oxidant exposure contributes to chondrocyte death over 24–48 hours after injuries involving a severe impact in a wide radius around impact sites (14–16, 22). Protection from this secondary phase of intracellular oxidation in vitro by rotenone, a well-known inhibitor of complex I of ETCs, or *N*-acetylcysteine (NAC), a nonspecific thiol antioxidant, suggests

exaggerated or aberrant activation of normal load-responsive mitochondrial redox pathways in chondrocytes after impact injuries (11, 14, 22). This injury pathway is likely to be compounded after IAFs where articular chondrocytes can be exposed to iron-rich, and therefore oxidizing, blood and ambient oxygen.

Despite demonstrating promise in mitigating articular responses to impact, rotenone's irreversible binding to complex I risks cytotoxicity and raises reasonable concerns regarding the safety of the treatment in humans. To address this concern, the barbiturate amobarbital, a reversible inhibitor of complex I (23), was substituted for rotenone. The study presented here is thus the penultimate preclinical effort at translating previous in vitro bovine and in vivo lapine (rabbit) studies of posttraumatic mitochondrial responses (24) into a clinically realistic large animal model of PTOA. The recently characterized minipig hock (ankle) IAF model is an excellent surrogate for human IAFs in terms of overall joint anatomy, inflammatory response, bone healing rate, and return to activity times (25). This unique translational vehicle allows a controlled, closed-joint, impact-induced IAF injury that is created with similar fracture energies encountered in human pilon fractures (26). In addition, the minipig hock IAF model is readily amenable to surgical fixation strategies that closely mimic human procedures. After injury, animals develop macroscopically apparent disease by 6 months on both the talus and tibia; further, much like the human analog (pilon fractures), even with high quality anatomic reduction of the IAF, the rate of disease is extremely high (5–8). Therapeutic efficacy in this large animal setting would indicate a strong candidacy for prospective clinical trials in humans. Therefore, this study was designed to test the hypothesis that administration of amobarbital or NAC after IAF and ORIF will provide significant therapeutic benefits to cartilage.

Results

Amobarbital inhibits ETC complex I in chondrocytes

To confirm the inhibition of complex I by amobarbital, we lysed primary chondrocytes freshly extracted from bovine articular cartilage and assayed them for complex I activity in the presence of increasing concentrations of amobarbital, yielding a dose dependent inhibition of complex I (Fig. 1A) not observed with similar measurements conducted on the other ETC complexes (fig. S1). These inhibitory effects were confirmed in intact chondrocytes plated for extracellular flux measurements, revealing a similar inhibition of oxygen consumption by amobarbital (Fig. 1B). These data support the idea that amobarbital can serve as a nontoxic alternative to rotenone for interrupting electron transport after mechanical injury. Surgical discards from human radial head IAFs cultured with 2.5 mM amobarbital displayed no differences in viable cell density indicated by Calcein AM staining after 3 days of culture compared to untreated controls (Fig. 1C–E). Note that these surgical discards were taken from patient procedures up to 1 week after IAF, beyond the proposed window for protection by amobarbital; thus we expect no additional cell death after harvest and therefore no change in viability with amobarbital. Data indicate that amobarbital is nontoxic to injured human articular cartilage at the doses used. Increasing amobarbital concentrations to 5 mM in this setting did not affect Calcein AM staining but began to incur

deficits in total adenosine 5'-triphosphate (ATP) concentration at 5 mM that may indicate a ceiling for therapeutic implementation (Fig. 1 F and G).

Early administration of amobarbital or NAC protects against PTOA

Directly after Yucatan minipig IAF and completion of ORIF, either 2.5 mM amobarbital (n = 5 with the exception of the tibial histology where n = 4) or 10 mM NAC (n = 6) suspended in a reverse thermal hydrogel vehicle was delivered via intra-articular injection. This hydrogel can be delivered in a liquid state that gels once introduced to physiological temperatures, facilitating injection and retention of the gel within the synovial joint. Standard blood chemistry analyses taken at surgery or harvest of amobarbital-treated animals indicated no significant changes or indications of toxicity (lowest $P = 0.91$, fig. S2). Macroscopic PTOA lesions were present on the tibia (Fig. 2A, scored in B) and concentrated on the talus (Fig. 2C, scored in D) after reproducible distal tibial fracture, as previously described (25). These were prevented at 6 months with amobarbital (n = 5 with the exception of the tibial histology where n = 4) or 10 mM NAC (n = 6). Articular cartilage from treated animals had a smoother appearance and a trend in the reduction in the number of macroscopic cartilage lesions at 6 months ($P = 0.16$ for amobarbital) that reached significance 12 months after amobarbital treatment ($P = 0.04$, fig. S3). Using previously published algorithms (25), automated histological quantitation of the weight-bearing areas of both the talar and tibial surfaces demonstrated significant reductions in average Mankin scores ($P < 0.05$), indicating less severe disease, by either treatment across the loaded area (Fig. 2B and D). Early cohorts included NAC animals that received a small pellet of poly(lactic-co-glycolic) acid (PLGA) encapsulated NAC at the time of surgery for extended release over ~2 weeks after injury in addition to the NAC dissolved in the hydrogel (fig. S4); however, after observing no differences between the extended release NAC group and the hydrogel NAC groups, and given the expense and duration of the studies, we subsequently pooled all NAC-receiving animals.

As controls we included both sham animals (n = 5), receiving all surgical procedures and internal hardware with the exception of the fracture-inducing impact, as well as naïve (normal) animals (n = 5). Pain scores on a scale from 0 to 4 were given during recovery and returned to normal around 4 weeks after ORIF (fig. S5). These scores indicated that the NAC animals may have had more discomfort during recovery, however NAC-treated animals still returned to baseline around the same time as the other groups. We hypothesize that this prolonged discomfort may be a result of the PLGA pellet within the joint of some of these animals. Pain scores indicated that ORIF animals had significantly more pain after 6 months than the NAC-and amobarbital-treated animals ($P < 0.05$), and sham animals show pain at 6 months exceeding the two treatment groups as well.

To further study progression of disease in this model, we took a cohort of amobarbital-treated animals to 12 months after IAF. Maximum and average Mankin scores trended lower in tissue from animals who received amobarbital treatment (n = 7) compared to controls (n = 6) (Fig. 3A and B, quantified in C and D). Talar tissue protected with amobarbital had begun to show early signs of disease at 6 months, whereas tibial tissue showed a trend toward improvement ($P = 0.12$). This diminished protection is complicated by a similar rise in

automated Mankin scores among the sham surgical animals, rendering talar differences between groups statistically insignificant and suggesting a meaningful contribution to PTOA from the surgical techniques and implantation of internal hardware. When synovial thickness at either time was examined, this contribution of sham surgery to disease was apparent at both 6 and 12 months with significant increases compared to normal porcine synovia ($P < 0.01$; Fig. 3E). By 12 months, sham ($P < 0.05$) and ORIF ($P < 0.05$) synovial thickness remained significantly different from normal, whereas neither amobarbital-treated ($P = 0.51$) nor NAC-treated ($P = 0.84$) groups increased significantly. Last, subchondral bone thickness at 6 months trended thinner in the ORIF group at the anterior talus and tibia ($P = 0.10$), where lesions were concentrated, further supporting the presence of the rapidly progressing PTOA phenotype in the ORIF group (Fig. 3F). By 12 months groups were not significantly different, and SDs had increased within groups, suggesting varying degrees of remodeling (ORIF versus sham $P = 0.57$; amobarbital versus sham $P = 0.56$; ORIF versus amobarbital $P = 0.57$, fig S6).

Oxidative stress and downstream responses by Nrf2 after IAF are prevented with NAC

Because NAC is readily taken up by cells and rapidly supplements the intracellular thiols oxidized by mechanical injury (11, 20), it represents a strong candidate for translation– as well as for testing whether the treatment effects observed could be derived from an antioxidant rather than an inhibitor of mitochondrial activity. In articular tissue harvested 1 week after IAF, we verified that NAC treatment increased total glutathione (GSH) (n = 10 for ORIF and n = 7 for ORIF + NAC; Fig. 4A). We observed an increase in total GSH alongside an increase in oxidation of GSH to GSSG with IAF (Fig. 4A and B) that suggests both oxidative stress and activation of the responsive transcription factor Nrf2, which contributes to the regulation of intracellular thiol content, after IAF. This was confirmed by stabilization of Nrf2 using immunohistochemistry (IHC) and nuclear localization using immunofluorescent techniques costained with 4’,6-diamidino-2-phenylindole (DAPI) (representative images with average positive cell counts per field inset; Fig. 4C). Administration of NAC at the time of injury prevented stabilization of the Nrf2 protein (n = 4 for all groups; Fig. 4C). Live chondrocytes harvested from these animals for standard XF96 extracellular flux mitochondrial stress tests demonstrated significant increases in proton leakage by mitochondrial membranes ($P < 0.05$), a further indication of oxidative stress with IAF that was prevented by NAC ($P < 0.05$; n = 10 for ORIF; and n = 7 for ORIF + NAC; Fig. 4D). To confirm that our amobarbital treatment was also active against proton leak at 1 week after impact, live rabbit chondrocytes harvested 1 week after 2 J impacts also showed increased proton leakage that could be prevented with early amobarbital treatment (Fig. 4E). Last, to demonstrate the presence of this pathway in less severe injuries and its responsiveness to other emerging therapeutics, we used a previously characterized modest meniscal injury model known to show mitochondrial dysfunction and proton leak at 1 month after injury was used (24). Rabbit chondrocytes harvested 1 week after rapamycin injection (administered 3 weeks after injury) confirmed that proton leak associated with meniscal injury was subverted (fig. S7). Rapamycin is a mitochondrial autophagy activator known to diminish arthritis (18).

Increases in proton leakage suggest that lipid peroxidation may be occurring in mitochondrial membranes. Using bovine osteochondral explants struck with a reproducible 2 J impact, we observed a significant decrease in mitochondrial staining of live cells within the impact site using MitoTracker Deep Red 24 hours after impact ($P < 0.01$, Fig. 5A and B). This decrease was exacerbated by culturing the explant in 21% O_2, supporting the hypothesis that this loss of mitochondria was oxygen-dependent. Preincubation with high concentrations of α-tocopherol acetate, a deliverable form of the lipid peroxidation chain-breaking antioxidant vitamin E, significantly protected against this loss of mitochondria ($P < 0.01$, Fig. 5B and C). Because 24 hour α-tocopherol treatment appeared to increase mitochondrial content, we added trolox (6-hydroxy-2,5,7,8-tetramethylchroman-2-carboxylic acid), a more soluble form of α-tocopherol, 1 hour before impact. We observed similar protection to the other treatments used. To further probe the mechanism leading to this loss of mitochondrial content, we added 2.5 mM dimethyl succinate or 2.5 mM dimethyl malonate to provide exogenous stimulation or inhibition, respectively, of the ETC through succinate dehydrogenase. Dimethyl succinate increased cell death and decreased mitochondrial content similarly to 21% oxygen, whereas dimethyl malonate provided a modest protection from injury but required continuous treatment after injury. This suggests that electron transport through succinate dehydrogenase plays a role in injury after IAF, but further study is necessary to delineate precise contributions from individual complexes.

The cohort of 1 week after IAF minipigs presented an opportunity to determine whether NAC provided any anti-inflammatory benefits in conjunction with its antioxidant properties. Indications of intracellular inflammation, as measured by full thickness immunohistochemical staining for p65 stabilization, were unchanged when quantified as cells staining positive for p65 (n = 4, Fig. 6A, quantified in Fig. 6B). A trend toward lower staining intensity and lower cell counts in the superficial zone of NAC treated hocks was noted during scoring but did not significantly affect overall per-cell staining compared to ORIF controls [$P = 0.47$ via two way analysis of variance (ANOVA)]; joint-wide indications of inflammation were similarly not significantly altered by NAC treatment relative to vehicle injections, including no changes in monocyte infiltration of the infrapatellar fat pad ($P = 0.38$ via two way ANOVA; scheme for analysis Fig. 6C; results Fig. 6D). Similarly, amobarbital had no impact on synovitis in rabbits receiving femoral impacts (n = 3; Fig. 6E), as analyzed 1 week after injury. These data suggest that the benefits of these treatments are not due to direct inhibition of joint inflammation.

Chondrocytes in treated hocks provide healthy anabolic activity after 6 months

After 6 months of normal activity after IAF, articular tissue was analyzed for proteoglycan (PG) content and mitochondrial energetic changes associated with PTOA (11, 19). The benefits of amobarbital and NAC, 6 months after any treatments were applied, included stronger safranin O staining for PG throughout the entire depth of the cartilage and within each zone, as quantified by our automated routine (n as described in Figs. 2 and 7, A and B). Statistically significant decreases in the ORIF group compared to all other groups ($P < 0.01$) demonstrated that improvements in Mankin score are a result of preventing structural degeneration (as shown in Fig. 1), as well as protection of chondrocyte anabolic processes critical to maintaining PG content. Mitochondrial stress tests reveal that basal (Fig. 7C) and

uncoupled maximal (Fig. 7D) oxygen consumption rates (OCRs) were increased in the cells isolated from IAF animals, similar to previously published results with chondrocytes harvested from osteoarthritic patients (11, 19). This effect was prevented to varying degrees with either NAC or amobarbital treatments. We also noted that proton leakage, similar to previous observations from human arthritic tissue (11, 19), was present 6 months after IAF, was not present in cells isolated from animals receiving either NAC or amobarbital (Fig. 7E).

Discussion

Mitochondrial ETC activity is increased after mechanical load in vitro (16, 17), and these mitochondria exhibit altered, often impaired, functionality after mechanical injury as a result of overload (10, 11, 13, 27); however, the extremely low oxygen tension of articular joints at baseline (28), low number of mitochondria per-cell (29), and strong dependence of chondrocytes upon glucose for energy (30, 31) have been taken to suggest that mitochondria likely have, at most, a minor role in PTOA development. On the contrary, here we have presented data supporting our hypothesis that strategies designed around mitochondrial responses to injury and developed to protect articular cartilage and resident chondrocytes in vitro can be translated into disease-modifying therapies for PTOA. This IAF treatment strategy targets the simultaneous stimulation of mitochondrial ETC activity by mechanical injury and exposure to high concentrations of blood and oxygen, known in vivo contributors to PTOA even in the absence of impact (32), into the normally avascular joint space via IAF. This combination of mechanical stimulation with a sudden excess of oxygen and other oxidants appears to represent ideal conditions for rendering the surviving articular chondrocytes unable to maintain the articular surface. Although this study cannot distinguish whether the benefits of NAC and amobarbital derived from prevention of cell death, prevention of subsequent alarmin release and signaling responses, or protection of surviving cell metabolic machinery, we deem it likely that all play a significant role in the treatments' efficacy. The proposed pathogenic pathway initiated by mechanical injury and exacerbated by mitochondrial dysfunction and its intersections with known elements of PTOA pathogenesis are summarized in fig. S8.

The importance of protecting chondrocytes after trauma to prevent subsequent development of PTOA has been a topic of debate in the orthopedic literature, with estimates of cell death varying between models and types of injury (4, 9, 33–37). Recently Heinemeier *et al.* (38) showed that once humans reach skeletal maturity the articular cartilage collagen matrix is essentially a permanent structure with no significant turnover even in the presence of osteoarthritic disease, whereas glycosaminoglycans turn over rapidly (38). This lack of collagen turnover dovetails with findings that articular chondrocytes are unlikely to migrate to and repopulate areas of widespread cell death where the extracellular matrix is intact (39). The high glycosaminoglycan turnover observed by Heinemeier *et al.* suggests that maintenance of cartilage glycosaminoglycan, and thus mechanical behavior, over time is reliant on *de novo* chondrocytic production of these molecules, and underscores the critical nature of chondrocyte anabolic function to cartilage health. In the case of minipig IAF, we have not only prevented articular chondrocyte death after a severe impact, but also preserved the basal metabolic activities of these articular chondrocytes for months after injury. The

typical, relatively sparse cell numbers in articular cartilage, taken together with the results of the Heinemeier study, support the hypothesis that prevention of PTOA after an IAF will require maximal protection of both chondrocyte viability and function.

Redox biological manipulations used previously as well as in this study, reveal critical features of oxidative stress that need to be accounted for when designing therapeutic interventions. Previous work with MitoQ supports the hypothesis that this oxidative stress centers around the mitochondria, targeted in this study with amobarbital (15). The efficacy of NAC, a compound that supports thiol redox metabolism and GSH-using enzymes (11, 15), suggests peroxidases commonly supported by GSH are critical to oxidative stress responses. This is corroborated by experiments showing that pretreatment with high concentrations of α-tocopherol, which prevents lipid peroxidation chain reactions, provides benefit in vitro; however, it is important to note that dietary supplementation of vitamin E during osteoarthritis treatment has proven ineffective (40). α-Tocopherol may be a poor therapeutic for many reasons, including the 24 hours required in our experimentation for entry into cells on account of the compound's poor solubility, the apparent need for α-tocopherol acetate to be used for entry into cells, and the relatively small increases seen in humans after dietary supplementation [single digit micromolar (41) compared to the 200 μM used here]. Thus, it is important to underscore that α-tocopherol is used here as a well-characterized lipid peroxidation chain breaking antioxidant without other antioxidant activity in vitro. To that end, we have also included experiments using trolox, which contains the same active moiety as α-tocopherol, as further support that lipid peroxidation is critical to the mitochondrial pathology observed.

To probe the metabolic features of this pathway beyond those revealed by amobarbital, exogenous succinate and malonate were added to assess potential sources of electrons leading to oxidative stress after IAF. The efficacy of rotenone and amobarbital, known inhibitors of complex I, suggests a forward flow of electrons from complex I to complex III; however, their activity also blocks reverse electron transport (21). On the basis of increases in toxicity with exogenous succinate, succinate accumulation may not be the primary contributor to injury from mechanical impact, although the increase in cell death observed demonstrates that increased flow through succinate dehydrogenase can contribute to oxidative stress in the impact setting. Malonate supplementation provided a protective benefit, further suggesting that succinate dehydrogenase plays a role in contributing to this injury; however the degree of protection was not comparable to amobarbital, NAC, or α-tocopherol and required a 24 hour incubation period after injury that is distinct from the more acute application of malonate cited (21). More study is needed to delineate the precise contributions of the different complexes under controlled conditions in vivo and evaluate possible reverse electron transport; however, these data support a working model where chaotic flow of electrons among highly damaged ETCs produces ROS primarily as a result of forward flow.

Although our porcine model is a robust surrogate of human injury and is amenable to realistic surgical interventions (25), there are several limitations. After IAF, minipigs begin to load their joints along a similar time scale to humans but differences in biped and quadruped responses to IAF have not been explored. This experiment represented an ideal

situation in which the minipigs received treatment within an hour after injury; however, delivery vehicles are available that would allow clinical delivery of amobarbital or NAC before surgical fixation (42). Our foundational studies suggest that targeting this pathway is effective when applied within 4 hours of the initial injury (43), but a therapeutic window must be determined in human applications where all of the appropriate clinical variables are present. Thus, human investigation is necessary for more detailed parameters for dosing (timing, number of injections, and volume of injections).

We note that our 6 and 12 month data p oints in pigs exhibit pain and histologic disease that appear to correspond well to the 2–4 year time course in which symptomatic PTOA develops in an unfortunate subset of rapidly progressing patients sustaining high energy pilon fractures (7, 8). The high progression rate for most of human pilon fractures over longer time periods, coupled with our observation that the most IAF minipigs progress to PTOA without biological treatment, suggest that patients sustaining pilon fractures may have the most to gain from initial clinical trials going forward. Because our studies throughout the translation of this approach have focused on mechanically severe impact injuries such as IAFs, it is unclear how these pathways and treatments might function in more modest, subfracturing impact injuries like severe sprains that lead to increased PTOA risk; however, note that the rapamycin experiment in the rabbit model suggests coherence between the pathway described here and other injury settings (18).

Finally, sham animals receiving the entire surgical IAF procedure but without fracturing impacts developed pain at 6 months and noticeable deterioration of their cartilage by 12 months. Slower progressing PTOA after surgical manipulation of a large animal’s joint, with zero resultant mechanical abnormalities and minimal disturbance of the joint (with the exception of the implantation of the internal hardware), combined with the efficacy of targeting articular cartilage biology, suggests two powerful and distinct—but interrelated—contributors to PTOA. Ideally, further studies in this model system will enable detailed study of the cross-talk between articular cartilage and its surrounding tissues.

In summary, amobarbital and NAC protected cartilage health and mitigated PTOA throughout porcine joints after IAF. To capture the breadth of this effect, we have used well-described, custom automated scoring algorithms (24, 25, 44–46) to provide large scale quantitation of histological changes associated with PTOA spanning the synovium, the weight-bearing areas of both articular surfaces, and the subchondral bone. Intra-articular administration of NAC or amobarbital significantly abrogated PTOA after an IAF as shown by classic PTOA indicators including PG content, cartilage thickness, and structural damage scores as well as intracellular phenomena linked to PTOA such as oxidative stress (4, 10, 11, 15, 19, 47, 48) and altered mitochondrial metabolism (10, 11, 13, 14, 17–19, 24, 27, 49). This occurred in the absence of any overt anti-inflammatory effect during the acute phase, suggesting either a distinct, oxidation-dependent pathway contributing to rapid PTOA progression or an uncoupling of inflammation from rapid progression via protection against oxidation. This lack of impact upon inflammation may be critical to the value of these therapies, given the well-known deleterious results of inhibiting inflammation during fracture healing. Future studies should interrogate longitudinal changes in intracellular metabolism and inflammation after injury to extend the treatment window of NAC and

amobarbital and determine a combination therapy capable of blunting the response to surgery. Although the eventual appearance of disease after trauma indicates room for improvement, this should not detract from the widespread efficacy observed with either treatment. Interrupting aberrant mitochondrial activity or protecting chondrocytes from the resulting oxidative stress after IAF holds substantial promise for mitigating PTOA and preserving a patient's quality of life.

Materials and Methods

Study design

This study was designed to test whether the two major treatments representing our previous lines of in vitro research, amobarbital and NAC (acute or extended release), could blunt or prevent articular cartilage degeneration after IAF in a porcine hock model of IAF. Power analyses determined that an n = 5 was necessary to provide a greater than 80% chance to detect improvement in automated Mankin scoring based on our previous characterization of the model and associated PTOA (25). Given the expense and duration of these experiments, we decided to combine the NAC and NAC with extended release treatment groups after the first three animals in each group were analyzed because no significant difference was observed between these two NAC treatments. Including the 1-week, 6-months, and 12-months animals, a total of 75 Yucatan minipigs were used for this study. Normal, sham, ORIF, ORIF + amobarbital, and ORIF + NAC groups at the outset contained at least seven animals; however seven total animals were removed from the study. Data from five animals was removed because of health concerns unrelated to their IAF procedures and data from two animals were censored when it was found after euthanasia that a small portion of a fracture fixation screw protruded into the joint. In addition, six New Zealand White rabbits receiving 2 J impacts to their femoral condyles and eleven New Zealand White rabbits underwent destabilization of the medial meniscus procedures as previously described (24), and received 10 μM rapamycin 3 weeks after surgery. Criteria for stopping any study before completion included persistent lameness or any indications of discomfort from the animals after surgical recovery not controlled with analgesic treatment. None of the animals met these criteria. All animals were observed by trained personnel on a daily basis and given a score ranging from 0 to 4 during the acute recovery period until the animals were determined to be healthy enough for transport to long term housing facilities where they received daily monitoring without a pain score. In addition to the animal experimentation, in vitro experimentation includes: healthy bovine osteochondral explants harvested from the femoral condyle and impacted with 2 J to assess acute redox metabolic end points, mitochondrial stress responses and mitochondrial content; healthy bovine chondrocytes extracted from the loaded areas of bovine knees used for assessments of amobarbital's chemical activity; and human radial head fragments obtained as surgical discards after radial head fractures.

No outliers or other observations were removed on account of their deviation from the mean in any of the experimentation shown. Most end points were chosen at the outset to evaluate the presence of PTOA in the articular cartilage of these animals and thus include numerous histological end points and scoring as well as several biochemical end points associated with

disease. Outcomes related to synovial thickening, subchondral bone thickness, intracellular anabolic function and oxidative stress were included as the study progressed. Data were collected blindly and decoded only after analysis. Male and female pigs were evenly distributed among groups, although the study was not powered to detect differences between males and females.

Live chondrocyte isolation and tissue culture

For monolayer assays, fresh bovine stifles (knees) obtained intact from a local abattoir (Bud's Custom Meats) were dissected and digested in collagenase and pronase (0.1 mg/ml; Sigma-Aldrich) overnight. Chondrocytes were then plated after pelleting and resuspension in growth medium. Identical procedures were used for any human chondrocytes harvested from radial head fragments after surgical discard and used in monolayer. Only primary, unpassaged cells were used in this study. For cultures of fresh bovine chondrocytes as well as cultures of human and bovine osteochondral explants, tissues were maintained using a 50:50 mix of Dulbecco's modified Eagel's medium and F12 (Gibco), with 10% fetal bovine serum (Gibco) added. All cultures were maintained at 5% O_2 and 5% CO_2 with the specific exception of the experiment exposing articular tissue to 21% oxygen after impact.

Electron transport chain and oxymetric assays

Whole cell lysates suspended in phosphate buffer were analyzed via a DU800 spectrophotometer (Beckman Coulter), as previously described (50). Samples were exposed to 2.5 mM amobarbital (Valeant Pharmaceuticals North America) in culture medium and assayed with increasing concentration of amobarbital present in the assay reactions themselves. Samples assayed without amobarbital present for measurement confirm the reversible inhibition of complex I by amobarbital. All assays conducted in 1 ml total volume. Complex I activity was measured as the rate of rotenone-inhibitable NADH (reduced form of nicotinamide adenine dinucleotide) oxidation. Samples were assayed with or without rotenone (200 μg/ml; Sigma-Aldrich) in working buffer containing 25 mM potassium phosphate buffer, 5 mM magnesium chloride, 2 mM potassium cyanide, bovine serum albumin (BSA) (2.5 mg/ml), 0.13 mM NADH, antimycin A (200 μg/ml), and 7.5 mM coenzyme Q1 (all from Sigma-Aldrich). Complex II samples were incubated with or without succinate in 25 mM potassium phosphate buffer, 5 mM magnesium chloride, 2 mM potassium cyanide, and BSA (2.5 mg/ml) for 10 min at 30°C. After 10 minutes, antimycin A (200 μg/ml), rotenone (200 μg/ml), 5 mM 2,6-dichloroindophenol (Sigma-Aldrich), and 7.5 mM coenzyme Q1 were added. Complex III samples were assayed in 25 mM potassium phosphate buffer, 5 mM magnesium chloride, 2 mM potassium cyanide, BSA (2.5 mg/ml), 0.5 mM n-dodecyl β-maltoside, rotenone (200 μg/ml), 1.5 mM cytochrome c, and 3.5 mM coenzyme Q2 (all from Sigma-Aldrich). Complex IV samples were assayed in 25 mM potassium phosphate buffer, 0.5 mM n-dodecyl β-maltoside, and 1.5 mM reduced cytochrome c. To evaluate oxygen consumption in the presence of amobarbital by chondrocytes, 20,000 primary bovine chondrocytes per well were plated on XF96 Extracellular Flux Analyzer (Seahorse Bioscience, Agilent) plates; a basal rate was measured, cells were then subjected to different concentrations of amobarbital, and a second rate was measured.

Evaluation of amobarbital toxicity

In accordance with Institutional Review Board regulations, human surgical discards were obtained fresh from patients receiving radial head implants after intra-articular or near-articular fractures of the radial head. These discards are removed from patients at the time of definitive fracture fixation, between 3 and 6 days after fracture, so no treatment effects are expected. Explants were cut from the articular surface of the radial head and cultured for 3 days with or without 2.5 mM amobarbital in normal medium. Half of each explant was homogenized for ATP analyses and a second half was stained with Calcein AM (Invitrogen) for 30 min and imaged via an Olympus FV1000 confocal laser scanning microscope (Olympus America). ATP analyses were conducted with bioluminescence kits (Sigma-Aldrich) in common usage (51) and normalized to protein concentration as determined via BCA assay or DNA content determined spectrophotometrically.

Porcine IAF model

All animal procedures including rabbit and porcine models were conducted under the approval of the University of Iowa's Institutional Animal Care and Use Committee. Seventy five skeletally mature, 2 year old Yucatan minipigs of both genders were used. The porcine model (25) uses a severe impact to the bottom (caudal aspect) of the anesthetized animal's foot to fracture the distal tibia, followed by surgical ORIF of the fracture. A carefully oriented stress rising saw cut through the anterior tibial cortex ensures a controlled, reproducible IAF when an impaction pendulum drives the talus into the tibia with 40 J [schematic shown in (25)]. This creates a single distal tibia fracture fragment that is then anatomically reduced and fixed using plates and screws during an open surgical procedure identical to human fracture treatment (ORIF). The fractures were anatomically reduced and then plated as previously described (25) using a veterinary-grade 2.7-mm tibial plateau leveling osteotomy plate (VP4400.R3-2.7, DePuy Synthes). Intra-articular injections of vehicle alone, amobarbital, or NAC for the treatment groups were given after the ORIF procedure was completed, between 30–60 minutes after IAF for each animal depending on pendulum function as well as individual fixation and suturing durations. To control for the surgical procedure used to create these IAFs, sham surgical animals received the entire procedure with the exception of the fracture-inducing impact; this included internal hardware and a hydrogel vehicle injection without NAC or amobarbital.

For cartilage treatment after IAF, either NAC or amobarbital was dissolved in 0.5 ml of a reverse-thermal responsive hydrogel used for the local delivery (intra-articular injection) of 2.5 mM amobarbital or 10 mM NAC (39, 52, 53). Hydrogel was prepared by adding 17% (w/v) F-127 (Sigma-Aldrich), 0.2% (w/v) hyaluronate (Gel-One, Zimmer Inc.), and 26 mM $NaHCO_3$ under sterile conditions, tested for endotoxin using the Limulus amebocyte lysate assay (Lonza) before injection. After treatment, animals were casted in a fiberglass cast for 1 week and allowed to bear weight as tolerated. One week postoperatively, casts were removed, a second 0.5 ml injection of the appropriate treatment was given, and casts were replaced for up to three additional weeks.

During this recovery period, and in the days preceding euthanasia, animals were given a pain score ranging from 0 to 4. This score was assessed as follows: 0 appetite normal, full weight

bearing on IAF limb when standing, full to partial weight bearing on IAF limb when walking, IAF limb touches the floor greater than 75% of the time while under observation; 1 appetite normal, mostly full weight bearing on IAF limb when standing, partial weight bearing on limb when walking, IAF limb touches the floor at least 75% of the time while under observation, interacts with surroundings; 2 appetite normal, partial weight bearing on IAF limb when standing, partial weight bearing on IAF limb when walking, IAF limb touches the floor at least 50% of the time while under observation, interacts with surroundings; 3 appetite normal to slightly decreased, IAF limb is used more for balance when standing/walking ("toe-touches") than weight bearing, partial weight bearing on IAF limb at least 25% time while under observation, interacts with surroundings; however will spend more time laying down; 4 -Decreased appetite, will not stand or has difficulty standing, unwilling to move, nonweight bearing on IAF limb at all times and cannot ambulate around pen. After the final cast removal, animals were left undisturbed in group housing for the duration of the experiments and given normal access to food and water.

Histological preparation and quantitative Mankin scoring

After postmortem tissue harvest, the tibia and talus were split into medial and lateral compartments, fixed in formalin, decalcified, embedded in paraffin, and cut into 5-μm sections. As previously described (25), sagittal sections were analyzed from each joint through the apex of the medial and lateral talar domes, as well as through the deepest concavities on the medial and lateral distal tibia. Each section was costained with Weigert's hematoxylin and eosin (H&E), safranin O, and Fast Green (all from Sigma-Aldrich) then digitized on an Olympus VS110 virtual microscopy system (Olympus) through a 20× objective (383 nm per pixel image resolution). This created a whole-joint composite image that was analyzed using a custom automated Mankin scoring routine (25). This scoring routine assigns a Mankin score for cell density, PG density, and structural defects at every 0.5 mm tissue increment spanning the full articular surface. Score are assigned on the basis of comparison of cell, structural, and image intensity information automatically quantified via image analysis techniques with reference values defined from normal Yucatan minipig hocks. These scores are then averaged over the full length of the articular surface being analyzed in a manner that approximates modern histological scoring for arthritis [Osteoarthritis Research Society International scores (44, 45)] within the Mankin rubric (46). A standardized 20-mm span of weight-bearing cartilage was evaluated on the talar and tibial surfaces. The automated scoring routines used here also delineated cartilage thickness and the zones of cartilage, allowing quantification of local PG content from safranin O intensities in each zone.

Extended release NAC preparation and validation

NAC loaded pellets [containing 70% polymer, 30% NAC (Sigma-Aldrich), and 10% plasticizer by weight] were produced using hot melt extrusion. The particle size of PLGA (50:50; 0.38 dl/g; Absorbable Polymers International) was reduced by grinding in a laboratory-scale grinder until it was the consistency of a fine powder. The PLGA and NAC were mixed in geometric proportions. The mixture was triturated with a pestle to form a uniform mixture for 10 min, and subsequently manually granulated with 10% polyethylene glycol (MW 375) for 10 min. The mixture was loaded into a Dynisco extruder hopper and

the pellets were extruded at 90 °C at a feeding rate of 200 mg/min, through a 1/16 inch die circular orifice. After cooling down, the extruded strands of NAC-loaded polymer were cut into pellets weighing 36 mg. The pellets were sterilized by 12 kilogray gamma radiation. The release of NAC from the pellets was measured in phosphate-buffered saline (PBS) by keeping them in an incubator shaker at 37 °C and 300 rpm. At each time point, the PBS was removed from the pellet and replaced with fresh PBS. The amount of NAC released at each time point was determined using Ellman's reagent [5,5-dithio-bis-(2-nitrobenzoic acid); Sigma-Aldrich] followed by spectrophotometric detection of reduction by NAC at 412 nm.

Oxidative stress measurements

GSH and GSSG were assayed using methods published by Griffith (54). Briefly, samples were minced in 5% sulfosalicylic acid and then subjected to three freeze-thaw cycles to ensure that all cells were lysed. Samples were then added to a buffer containing dithionitrobenzoic acid (DTNB), GSH reductase and excess NADPH (reduced form of nicotinamide adenine dinucleotide phosphate) (all from Sigma-Aldrich). Reduced GSH molecules react with the DTNB to produce a yellow product, whereupon GSH reductase recycles the GSH. Thus, the rate of absorbance change at 412 nm is proportional to GSH concentration in a relationship determined by standard curve. To measure GSSG, 20% of sample volume of 2-vinylpyridine (Sigma-Aldrich) was added to a sample aliquot for 1 hour before analyses rendering reduced GSH unavailable for recycling.

Nrf2 and p65 IHC was conducted using previously published IHC techniques (39). Briefly, after paraffin embedding and sectioning at 5 μm, samples were stained with primary antibody, anti-Nrf2 (Abcam) or anti-p65 (Abcam), at a dilution of 1:50 for Nrf2 and 1:100 for p65 overnight. In the morning, slides were rinsed with PBS and blocked for 30 min with goat serum and BSA (Gibco), and secondary (goat anti-rabbit) was added (1:250) for 30 min. Secondary was visualized using standard ABC and DAB reagents (Abcam), and slides were scanned using the components detailed for Mankin scoring above. For immunofluorescence (IF), similar protocols to previous studies were used (39); however, visualization was carried out through a goat anti-rabbit secondary conjugated with Alexa Fluor 568 (Thermo Fisher Scientific) and DAPI staining. Slides were imaged via an Olympus FV1000 confocal laser scanning microscope. Quantitation of cell positivity for either IHC or IF was carried out by counting positive cells per 20X objective field and comparing that to the total cell number.

Extracellular flux assays

To determine basal OCR, maximum OCR, and proton leakage rates, standard mitochondrial stress tests were conducted using an XF96 Extracellular Flux Analyzer (Seahorse Bioscience, Agilent) as previously described (11). Injections contained: 2 μM oligomycin, 250 nM FCCP, 2 μM rotenone and 5 μM antimycin A (all from Sigma-Aldrich). OCRs were normalized to cell number as counted via hemocytometer after trypsinization. Proton leakage rates were normalized to basal OCRs of each individual sample.

Synovial inflammation and monocyte infiltration

The posterior joint capsule was excised and processed into 5 μm thick axial histological sections and stained with H&E. Slides were digitized on the Olympus VS110 digital histology system as described above for Mankin scoring. Images from the 1-week survival minipigs were imported into Visiomorph software (Visiopharm) for analysis of synovial inflammation using an automated routine. Within the user defined area, cell nuclei were automatically identified within the adipose tissue based on color thresholds, and monocytes were separated from adipocytes based on nuclear aspect ratio. Monocyte count was converted to monocyte density by dividing the cell number by the area of tissue analyzed. In the synovial tissue harvested 6 and 12 months after IAF, the adipose tissue was fully fibrosed and synovial thickening had to be measured manually. For these specimens, measurement tools included in the software used to run the digital image acquisition (VS-ASW, Olympus) were used to manually measure the thickness of the synovial tissue at five locations distributed over the full tissue section. These five replicate measurements were averaged to obtain a single thickness measurement for each section. Subchondral bone thickness measurements were made manually using the software-based measurement tools at anterior, middle, and posterior locations on the same sagittal histological images used to derive the Mankin scores.

Live cell analysis of mitochondrial content

Assessment of bovine osteochondral explants for total mitochondrial content after impact was carried out using 200 nM MitoTracker Deep Red (Invitrogen) for 30 min. Live cell staining and imaging (costained with Calcein AM) were identical to the human staining above. Images within an area impacted with 2 J via 1 kg drop tower (14) were captured via an Olympus confocal microscope using a 4× or 10× objective and ImageJ was used to quantify average intensity in the damaged area. Treatments applied individually to culture medium after impact only included 2.5 mM amobarbital and 10 mM NAC. For experiments using 200 μM α-tocopherol, α-tocopherol acetate (Sigma-Aldrich) was used to facilitate entry into cells; explants were treated 24 hours before impact and 24 hours after impact. Treatments preloaded 1 hour before impact included 200 μM trolox, 2.5 mM dimethylmalonate, 2.5 mM dimethyl succinate (all from Sigma-Aldrich).

Statistical analyses

For all experimentation shown, error bars indicate SDs. All statistical analyses were completed using GraphPad Prism 7. $P < 0.05$ was used to determine significance except where otherwise noted. Column comparisons shown in Figs. 1 and 5 indicate one way ANOVA. Comparisons in Fig. 4 indicate two sided Student's t-test between the noted groups and control and pain score differences at 6 months shown in fig. S5 were compared using a χ^2 analysis. Differences noted in Figs. 2, 3 and 7 were determined with two-way ANOVA including treatments and normal and sham animals where appropriate followed by posttesting using Dunnett's test to compare the effects of multiple treatments. Monocyte infiltration data and proportions of cells staining positive for p65 from Fig. 6 were tested using two sided Student's t-tests between hydrogel and NAC/glycyrrhizin-treated groups and untreated groups and no significant differences were found.

Supplementary Material

Refer to Web version on PubMed Central for supplementary material.

Acknowledgments

Funding: We would like to acknowledge the generous support of the Department of Defense (#W81XWH-11-1-0583 and W81XWH-10-1-0864) and the NIH (CORT: 5 P50 AR055533-05). We also acknowledge the Orthopedic Trauma Association (no. 245) for their support.

References and Notes

1. Brown TD, Johnston RC, Saltzman CL, Marsh JL, Buckwalter JA. Posttraumatic osteoarthritis: a first estimate of incidence, prevalence, and burden of disease. J Orthop Trauma. 2006 Nov-Dec; 20(10):739–44. [PubMed: 17106388]
2. Rivera JC, Wenke JC, Buckwalter JA, Ficke JR, Johnson AE. Posttraumatic osteoarthritis caused by battlefield injuries: the primary source of disability in warriors. J Am Acad Orthop Surg. 2012; 20(suppl 1):S64–9. [PubMed: 22865140]
3. Praemer, A., Furner, S., Furner, RD. The Burden of Musculoskeletal Diseases in the United States: Prevalence, Societal and Economic Cost. AAOS; 1999.
4. McKinley TO, Borrelli J Jr, D'Lima DD, Furman BD, Giannoudis PV. Basic science of intra-articular fractures and posttraumatic osteoarthritis. J Orthop Trauma. 2010 Sep; 24(9):567–70. [PubMed: 20736796]
5. Marsh JL, Buckwalter JA, Gelberman R, Dirschl D, Olson S, Brown T, Llinias A. Articular fractures: does an anatomic reduction really change the result? J Bone Joint Surg Am. 2002 Jul; 84-a(7):1259–71. [PubMed: 12107331]
6. Matta JM. Fractures of the acetabulum: accuracy of reduction and clinical results in patients managed operatively within three weeks after the injury. J Bone Joint Surg Am. 1996 Nov; 78(11): 1632–45. [PubMed: 8934477]
7. Honkonen SE. Degenerative arthritis after tibial plateau fractures. J Orthop Trauma. 1995; 9(4):273–7. [PubMed: 7562147]
8. Marsh JL, Weigel DP, Dirschl DR. Tibial plafond fractures. How do these ankles function over time? J Bone Joint Surg Am. 2003 Feb; 85-a(2):287–95. [PubMed: 12571307]
9. Anderson DD, Chubinskaya S, Guilak F, Martin JA, Oegema TR, Olson SA, Buckwalter JA. Post-traumatic osteoarthritis: improved understanding and opportunities for early intervention. J Orthop Res. 2011 Jun; 29(6):802–9. [PubMed: 21520254]
10. Koike M, Nojiri H, Ozawa Y, Watanabe K, Muramatsu Y, Kaneko H, Morikawa D, Kobayashi K, Saita Y, Sasho T, Shirasawa T, Yokote K, Kaneko K, Shimizu T. Mechanical overloading causes mitochondrial superoxide and SOD2 imbalance in chondrocytes resulting in cartilage degeneration. Sci Rep. 2015 Jun 25.5:11722. [PubMed: 26108578]
11. Coleman MC, Ramakrishnan PS, Brouillette MJ, Martin JA. Injurious loading of articular cartilage compromises chondrocyte respiratory function. Arthritis Rheumatol. 2016; 68:662–71. [PubMed: 26473613]
12. Lee RB, Urban JP. Functional replacement of oxygen by other oxidants in articular cartilage. Arthritis Rheum. 2002 Dec; 46(12):3190–200. [PubMed: 12483723]
13. Lee RB, Wilkins RJ, Razaq S, Urban JP. The effect of mechanical stress on cartilage energy metabolism. Biorheology. 2002; 39(1–2):133–43. [PubMed: 12082276]
14. Goodwin W, McCabe D, Sauter E, Reese E, Walter M, Buckwalter JA, Martin JA. Rotenone prevents impact-induced chondrocyte death. J Orthop Res. 2010 Aug; 28(8):1057–63. [PubMed: 20108345]
15. Wolff KJ, Ramakrishnan PS, Brouillette MJ, Journot BJ, McKinley TO, Buckwalter JA, Martin JA. Mechanical stress and ATP synthesis are coupled by mitochondrial oxidants in articular cartilage. J Orthop Res. 2013 Feb; 31(2):191–6. [PubMed: 22930474]

16. Brouillette MJ, Ramakrishnan PS, Wagner VM, Sauter EE, Journot BJ, McKinley TO, Martin JA. Strain-dependent oxidant release in articular cartilage originates from mitochondria. Biomech Model Mechanobiol. 2014 Jun; 13(3):565–72. [PubMed: 23896937]
17. Terkeltaub R, Johnson K, Murphy A, Ghosh S. Invited review: the mitochondrion in osteoarthritis. Mitochondrion. 2002 Feb; 1(4):301–19. [PubMed: 16120285]
18. López de Figueroa P, Lotz MK, Blanco MKFJ, Caramés B. Autophagy activation and protection from mitochondrial dysfunction in human chondrocytes. Arthritis Rheumatol. 2015; 67(4):966–76. [PubMed: 25605458]
19. Gavriilidis C, Miwa S, von Zglinicki T, Taylor RW, Young DA. Mitochondrial dysfunction in osteoarthritis is associated with down-regulation of superoxide dismutase 2. Arthritis Rheum. 2013; 65(2):378–87. [PubMed: 23138846]
20. Ferreira R, Llesuy S, Milei J, Scordo D, Hourquebie H, Molteni L, de Palma C, Boveris A. Assessment of myocardial oxidative stress in patients after myocardial revascularization. Am Heart J. 1988 Feb; 115(2):307–12. [PubMed: 3341166]
21. Chouchani ET, Pell VR, Gaude E, Aksentijevic D, Sundier SY, Robb EL, Logan A, Nadtochiy SM, Ord EN, Smith AC, Eyassu F, Shirley R, Hu CH, Dare AJ, James AM, Rogatti S, Hartley RC, Eaton S, Costa AS, Brookes PS, Davidson SM, Duchen MR, Saeb-Parsy K, Shattock MJ, Robinson AJ, Work LM, Frezza C, Krieg T, Murphy MP. Ischaemic accumulation of succinate controls reperfusion injury through mitochondrial ROS. Nature. 2014 Nov 20; 515(7527):431–5. [PubMed: 25383517]
22. Martin JA, McCabe D, Walter M, Buckwalter JA, McKinley TO. N-acetylcysteine inhibits post-load chondrocyte death in osteochondral explants. J Bone Joint Surg Am. 2009; 91:1890–7. [PubMed: 19651946]
23. Bernofsky C, Mills RC. Diaphorases from Aerobacter aerogenes. J Bacteriol. 1966 Nov; 92(5): 1404–14. [PubMed: 5924271]
24. Goetz JE, Coleman MC, Fredericks DC, Petersen E, Martin JA, McKinley TO, Tochigi Y. Time-dependent loss of mitochondrial function precedes progressive histologic cartilage degeneration in a rabbit meniscal destabilization model. J Orthop Res. 2016 Jun 9.
25. Goetz JE, Fredericks D, Petersen E, Rudert MJ, Baer T, Swanson E, Roberts N, Martin JA, Tochigi Y. A clinically realistic large animal model of intra-articular fracture that progresses to post-traumatic osteoarthritis. Osteoarthritis Cartilage. 2015 Oct; 23(10):1797–805. [PubMed: 26033166]
26. Dibbern K, Kempton LB, Higgins TF, Morshed S, McKinley TO, Marsh JL, Anderson DD. Fractures of the tibial plateau involve similar energies as the tibial pilon but greater articular surface involvement. J Orthop Res. 2017 Mar; 35(3):618–624. [PubMed: 27381653]
27. Johnson K, Jung A, Murphy A, Andreyev A, Dykens J, Terkeltaub R. Mitochondrial oxidative phosphorylation is a downstream regulator of nitric oxide effects on chondrocyte matrix synthesis and mineralization. Arthritis Rheum. 2000 Jul; 43(7):1560–70. [PubMed: 10902761]
28. Lund-Olesen K. Oxygen tension in synovial fluids. Arthritis Rheum. 1970 Nov-Dec;13(6):769–76. [PubMed: 5495389]
29. Buckwalter JA, Mower D, Ungar R, Schaeffer J, Ginsberg B. Morphometric analysis of chondrocyte hypertrophy. J Bone Joint Surg Am. 1986 Feb; 68(2):243–55. [PubMed: 3944163]
30. Otte P. Basic cell metabolism of articular cartilage. Manometric studies. Z Rheumatol. 1991 Sep-Oct;50(5):304–12. [PubMed: 1776367]
31. Spencer CA, Palmer TN, Mason RM. Intermediary metabolism in the Swarm rat chondrosarcoma chondrocyte. Biochem J. 1990 Feb 1; 265(3):911–4. [PubMed: 2306225]
32. Myers SL, Brandt KD, O'Connor BL, Visco DM, Albrecht ME. Synovitis and osteoarthritic changes in canine articular cartilage after anterior cruciate ligament transection. Effect of surgical hemostasis. Arthritis Rheum. 1990 Sep; 33(9):1406–15. [PubMed: 2403403]
33. Novakofski KD, Berg LC, Bronzini I, Bonnevie ED, Poland SG, Bonassar LJ, Fortier LA. Joint-dependent response to impact and implications for post-traumatic osteoarthritis. Osteoarthritis Cartilage. 2015 Jul; 23(7):1130–7. [PubMed: 25725390]
34. Chubinskaya S, Wimmer MA. Key Pathways to Prevent Posttraumatic Arthritis for Future Molecule-Based Therapy. Cartilage. 2013 Jul; 4(3 Suppl):13S–21S. [PubMed: 26069661]

35. Hembree WC, Ward BD, Furman BD, Zura RD, Nichols LA, Guilak F, Olson SA. Viability and apoptosis of human chondrocytes in osteochondral fragments following joint trauma. J Bone Joint Surg Br. 2007 Oct; 89(10):1388–95. [PubMed: 17957084]
36. Ewers BJ, Dvoracek-Driksna D, Orth MW, Haut RC. The extent of matrix damage and chondrocyte death in mechanically traumatized articular cartilage explants depends on rate of loading. J Orthop Res. 2001 Sep; 19(5):779–84. [PubMed: 11562121]
37. Repo RU, Finlay JB. Survival of articular cartilage after controlled impact. J Bone Joint Surg Am. 1977 Dec; 59(8):1068–76. [PubMed: 591538]
38. Heinemeier KM, Schjerling P, Heinemeier J, Moller MB, Krogsgaard MR, Grum-Schwensen T, Petersen MM, Kjaer M. Radiocarbon dating reveals minimal collagen turnover in both healthy and osteoarthritic human cartilage. Sci Transl Med. 2016 Jul 6.8(346) 346ra90.
39. Yu Y, Brouillette MJ, Seol D, Zheng H, Buckwalter JA, Martin JA. Use of recombinant human stromal cell-derived factor 1α-loaded fibrin/hyaluronic acid hydrogel networks to achieve functional repair of full-thickness bovine articular cartilage via homing of chondrogenic progenitor cells. Arthritis Rheumatol. 2015 May; 67(5):1274–85. [PubMed: 25623441]
40. Canter PH, Wider B, Ernst E. The antioxidant vitamins A, C, E and selenium in the treatment of arthritis: a systematic review of randomized clinical trials. *Rheumatology* (Oxford). 2007 Aug; 46(8):1223–33. [PubMed: 17522095]
41. Roxborough HE, Burton GW, Kelly FJ. Inter- and intra-individual variation in plasma and red blood cell vitamin E after supplementation. Free Radic Res. 2000 Oct; 33(4):437–45. [PubMed: 11022852]
42. Kim Y, Seol DR, Mohapatra S, Sunderland JJ, Schultz MK, Domann FE, Lim TH. Locally targeted delivery of a micron-size radiation therapy source using temperature-sensitive hydrogel. Int J Radiat Oncol Biol Phys. 2014 Apr 1; 88(5):1142–7. [PubMed: 24495593]
43. Martin JA, Anderson DD, Goetz JE, Fredericks D, Pedersen DR, Ayati BP, Marsh JL, Buckwalter JA. Complementary models reveal cellular responses to contact stresses that contribute to post-traumatic osteoarthritis. J Orthop Res. 2017 Mar; 35(3):515–523. [PubMed: 27509320]
44. Moussavi-Harami SF, Pedersen DR, Martin JA, Hillis SL, Brown TD. Automated objective scoring of histologically apparent cartilage degeneration using a custom image analysis program. J Orthop Res. 2009 Apr; 27(4):522–8. [PubMed: 18972361]
45. Pritzker KP, Gay S, Jimenez SA, Ostergaard K, Pelletier JP, Revell PA, Salter D, van den Berg WB. Osteoarthritis cartilage histopathology: grading and staging. Osteoarthritis Cartilage. 2006 Jan; 14(1):13–29. [PubMed: 16242352]
46. Mankin HJ, Dorfman H, Lippiello L, Zarins A. Biochemical and metabolic abnormalities in articular cartilage from osteo-arthritic human hips. II. Correlation of morphology with biochemical and metabolic data. J Bone Joint Surg Am. 1971 Apr; 53(3):523–37. [PubMed: 5580011]
47. Aruoma OI, Kaur H, Halliwell B. Oxygen free radicals and human diseases. J R Soc Health. 1991 Oct; 111(5):172–7. [PubMed: 1795351]
48. Abusarah J, Bentz M, Benabdoune H, Rondon PE, Shi Q, Fernandes JC, Fahmi H, Benderdour M. Inflamm Res. 2017 Oct; 66(8):637–651. [PubMed: 28447122]
49. Martin JA, Martini A, Molinari A, Morgan W, Ramalingam W, Buckwalter JA, McKinley TO. Mitochondrial electron transport and glycolysis are coupled in articular cartilage. Osteoarthritis Cartilage. 2012 Apr; 20(4):323–9. [PubMed: 22305999]
50. Birch-Machin MA, Briggs HL, Saborido AA, Bindoff LA, Turnbull DM. An evaluation of the measurement of the activities of complexes I-IV in the respiratory chain of human skeletal muscle mitochondria. Biochem Med Metab Biol. 1994 Feb; 51(1):35–42. [PubMed: 8192914]
51. Long JA, Guthrie HD. Validation of a rapid, large-scale assay to quantify ATP concentration in spermatozoa. Theriogenology. 2006; 65:1620–1630. [PubMed: 16364417]
52. Lee J, Lim T, Park J. Intradiscal drug delivery system for the treatment of low back pain. J Biomed Mater Res A. 2010 Jan; 92(1):378–85. [PubMed: 19191317]
53. Seol D, Magnetta MJ, Ramakrishnan PS, Kurriger GL, Choe H, Jang K, Martin JA, Lim TH. Biocompatibility and preclinical feasibility tests of a temperature-sensitive hydrogel for the purpose of surgical wound pain control and cartilage repair. J Biomed Mater Res B Appl Biomater. 2013 Nov; 101(8):1508–15. [PubMed: 24591226]

54. Griffith OW. Determination of glutathione and glutathione disulfide using glutathione reductase and 2-vinylpyridine. Anal Biochem. 1980; 106:207–212. [PubMed: 7416462]

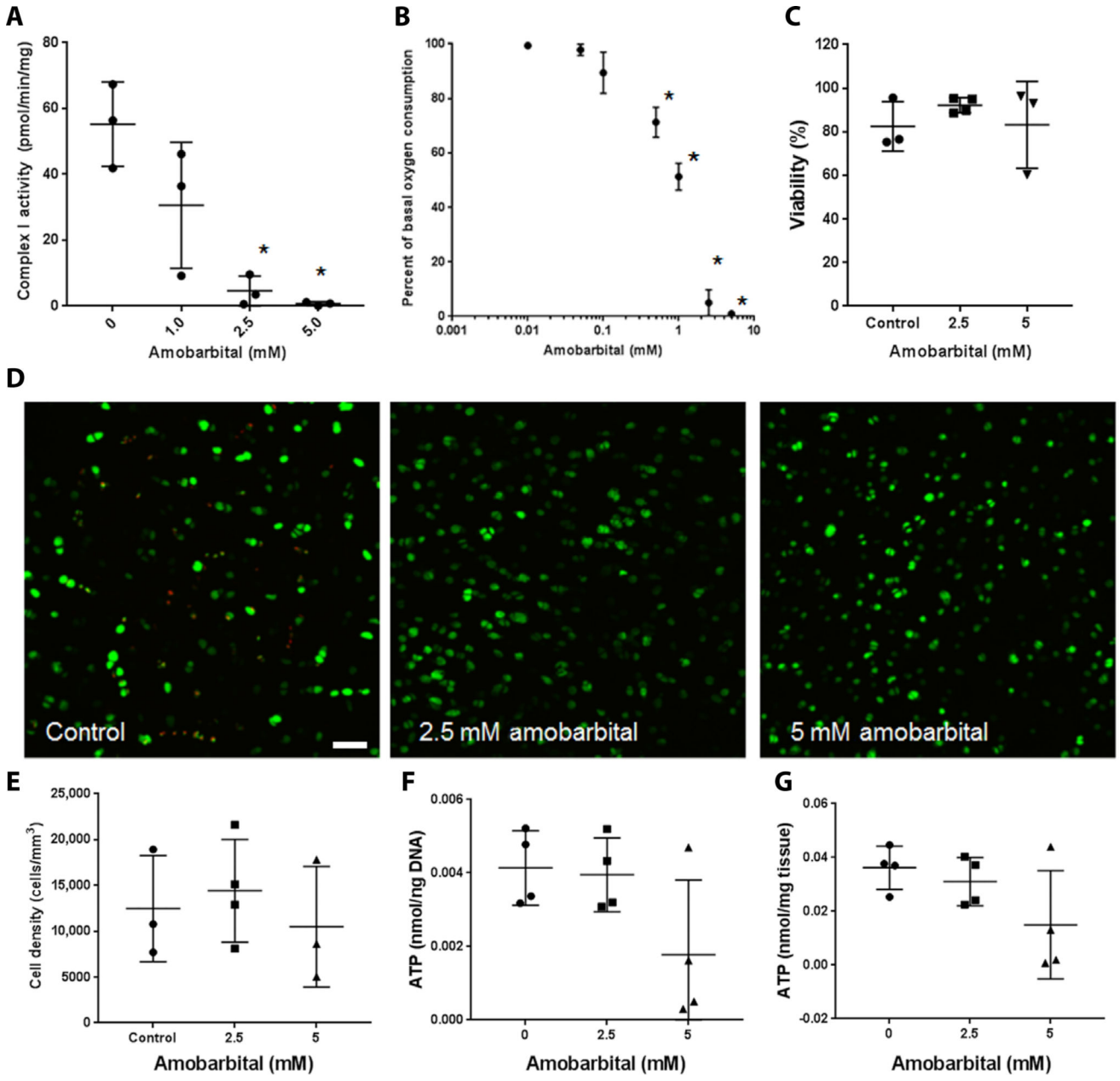

Fig. 1. Amobarbital inhibits chondrocyte complex I activity and is nontoxic to human chondrocytes at therapeutic doses

(**A**) Spectrophotometric assay of freshly harvested bovine articular chondrocyte NADH (reduced form of nicotinamide adenine dinucleotide) dehydrogenase activity in the presence of increasing concentrations of amobarbital [n = 3; * $P < 0.01$ versus control via one way analysis of variance (ANOVA)]. For each group and panel, lines indicate mean and SD. (**B**) Extracellular flux analysis of oxygen consumption rates in bovine chondrocyte monolayers in the presence of increasing concentrations of amobarbital (n = 3; * $P < 0.01$ versus control via one way ANOVA). Circles represent means. (**C**) Percent viability as indicated by Calcein AM positivity of human articular chondrocytes taken from human intra-articular fracture (IAF) discards and cultured as osteochondral explants in the presence of amobarbital for 3

days (n = 3 except 2.5 mM, where n = 4; no significant differences via one way ANOVA). (**D**) Representative images of Calcein AM stained human cartilage explants exposed to amobarbital (n = 3; * $P < 0.01$ versus control via one way ANOVA). Scale bar, 50 μm. (**E**) Quantitation of viable cell density within cartilage from Calcein AM images of human explants (n = 3; no statistical differences indicated by one way ANOVA). (**F**) Whole human cartilage adenosine 5'-triphosphate (ATP) concentration normalized to total DNA content after amobarbital exposure (n = 4; no differences indicated by one way ANOVA). (**G**) Whole human cartilage ATP concentration normalized to protein content after amobarbital exposure (n = 4; no differences indicated by one way ANOVA).

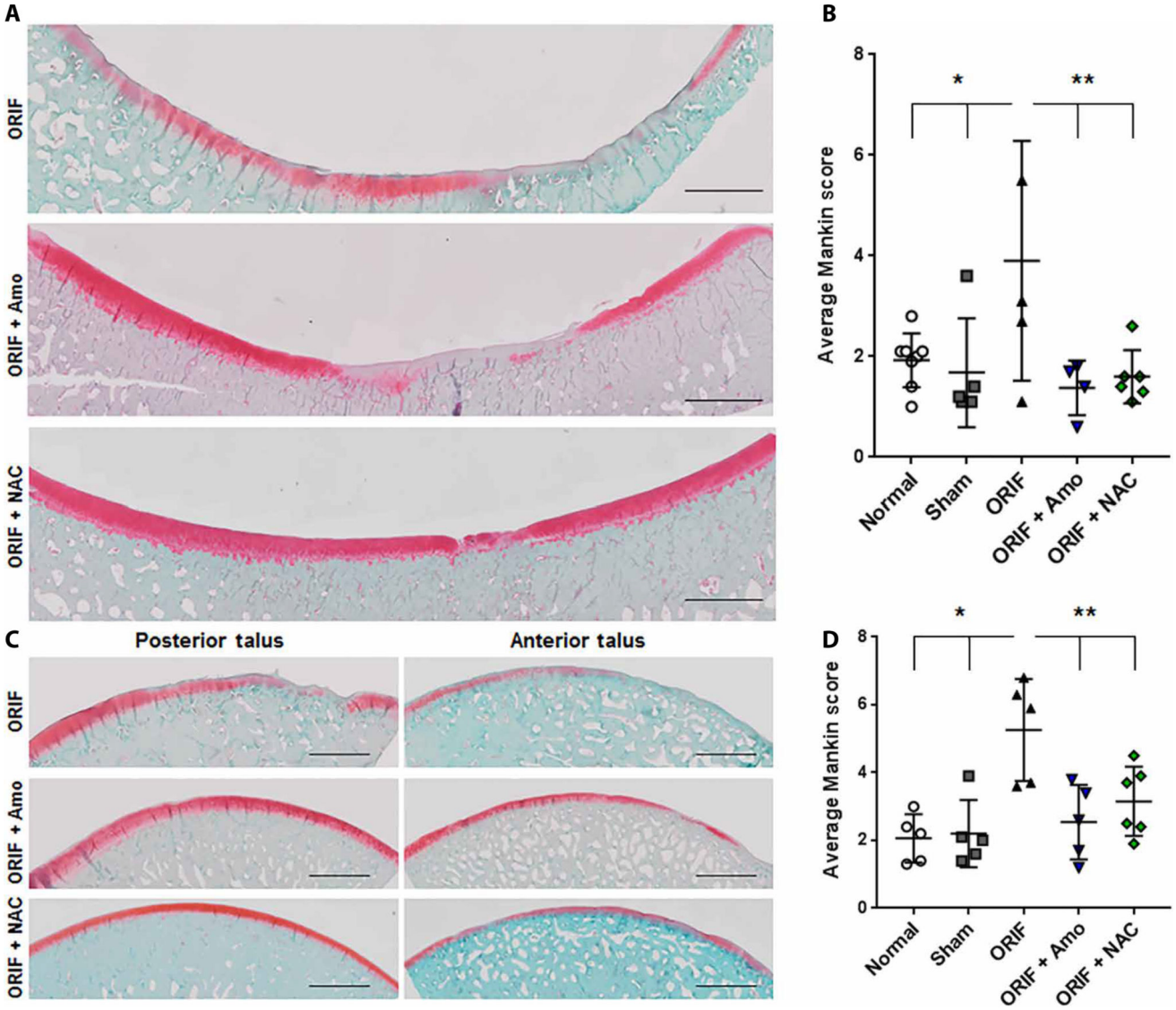

Fig. 2. Acute administration of amobarbital or NAC after IAF prevents PTOA development 6 months after IAF

(**A**) Representative images of the loaded portion of the porcine medial tibia stained for proteoglycan content via safranin O 6 months after fracture [n = 8 for normal, n = 5 for sham, n = 5 for open reduction and internal fixation (ORIF), n = 4 for ORIF + amobarbital (Amo), n = 6 for ORIF + *N*-acetylcysteine (NAC)]. Images are a composite of 20X scans across the entire anterior-posterior length of the surface. Scale bars, 2 mm. (**B**) Semi-automated Mankin scoring of the loaded areas of the medial tibia spanning both the anterior and posterior segments [n same as in (**A**); * $P < 0.05$ versus normal and sham; ** $P < 0.05$ versus ORIF; all via two way ANOVA with Dunnett's posttest). (**C**) Representative images of the loaded portions of the porcine medial talus stained for proteoglycan content via safranin O 6 months after fracture (n = 8 for normal, n = 5 for sham, n = 5 for ORIF, n = 5 for ORIF + amobarbital, and n = 6 for ORIF + NAC). Images are a composite of 20X scans across either the anterior or posterior (samples cut in half for staining) length of the talus.

Scale bars, 2 mm. (**D**) Semi-automated Mankin scoring of the loaded areas of the medial talus spanning both the anterior and posterior segments (n same as (**C**), * $P < 0.05$ versus normal and sham, ** $P < 0.05$ versus ORIF, all via two way ANOVA with Dunnett's post-test). Data represent the mean with SD shown.

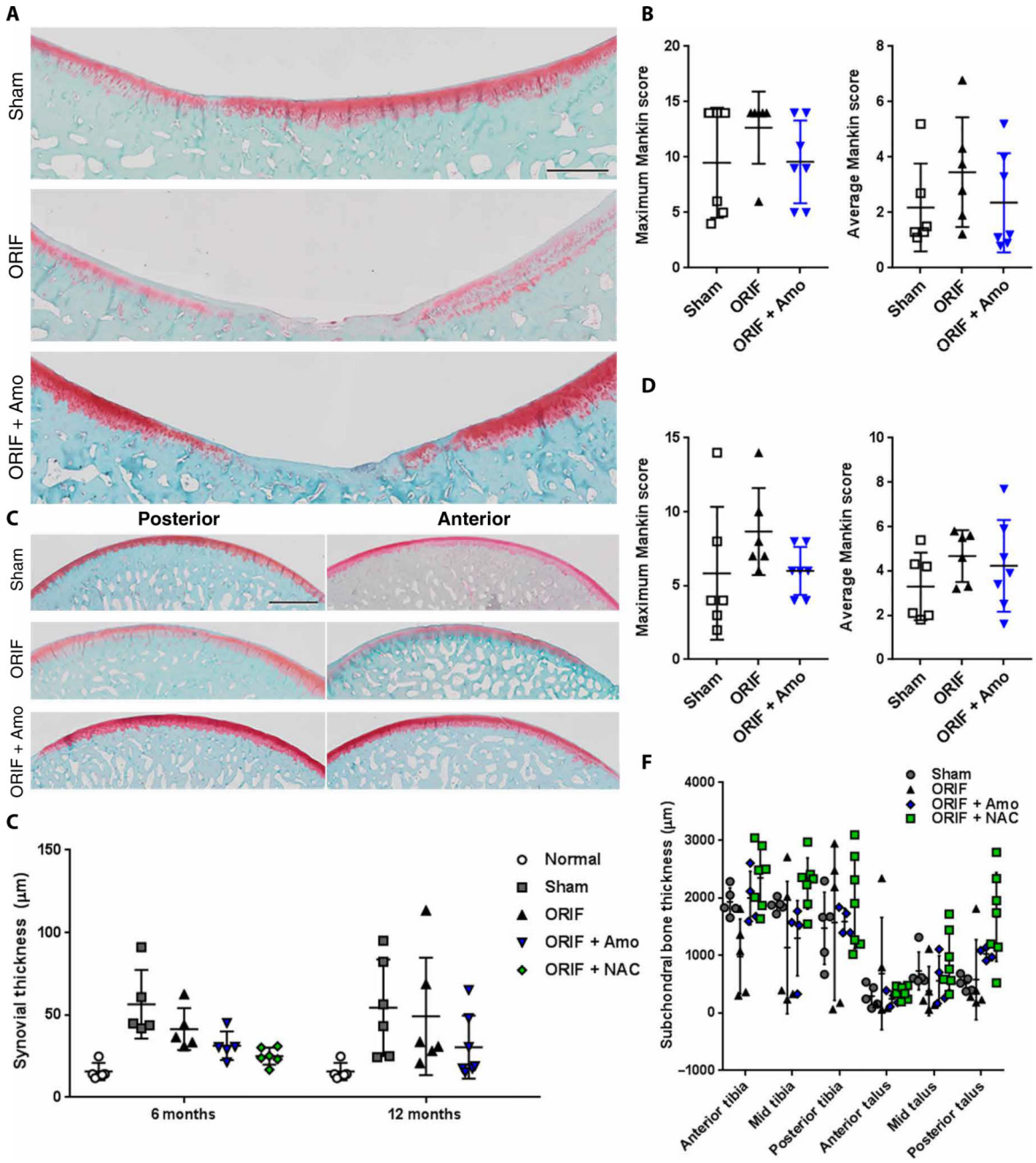

Fig. 3. Sham surgical procedures used for IAF modeling cause indications of PTOA by 12 months after ORIF

(**A**) Representative images of the loaded portion of the porcine medial tibia stained for proteoglycan content via safranin O 12 months after fracture (n = 6 for sham, n = 6 for ORIF, n = 7 for ORIF + amobarbital). Images are a composite of 20X scans across the entire anterior-posterior length of the surface. Scale bar, 2 mm. (**B**) Semiautomated Mankin scoring of the loaded areas of the porcine medial tibia spanning both the anterior and posterior segments, with maximum and average values given [n same as in (**A**); all $P > 0.05$ versus sham as indicated by two-way ANOVA with Dunnett's posttest]. (**C**) Representative

images of the loaded portions of the porcine medial talus stained for proteoglycan content via safranin O 12 months after fracture [n same as in (**A**)]. Images are a composite of 20X scans across either the anterior or posterior (samples cut in half for staining) length of the talus. Scale bar, 2 mm. (**D**) Semiautomated Mankin scoring of the loaded areas of the porcine medial talus spanning both the anterior and posterior segments, with maximum and average values given [n same as in (**A**)]. (**E**) Synovial thickness measured from the posterior portion of the capsule at 6 and 12 months [n as indicated in Fig. 2 or in (**A**) for 6 and 12 months, respectively; * $P < 0.05$ versus normal via two way ANOVA with Dunnett's posttest]. (**F**) Subchondral bone thickness at 6 months from micrographs used for Fig. 2 (n as indicated in Fig. 2, no significant difference found via two way ANOVA with Dunnett's posttest). Data represent the mean with SD shown.

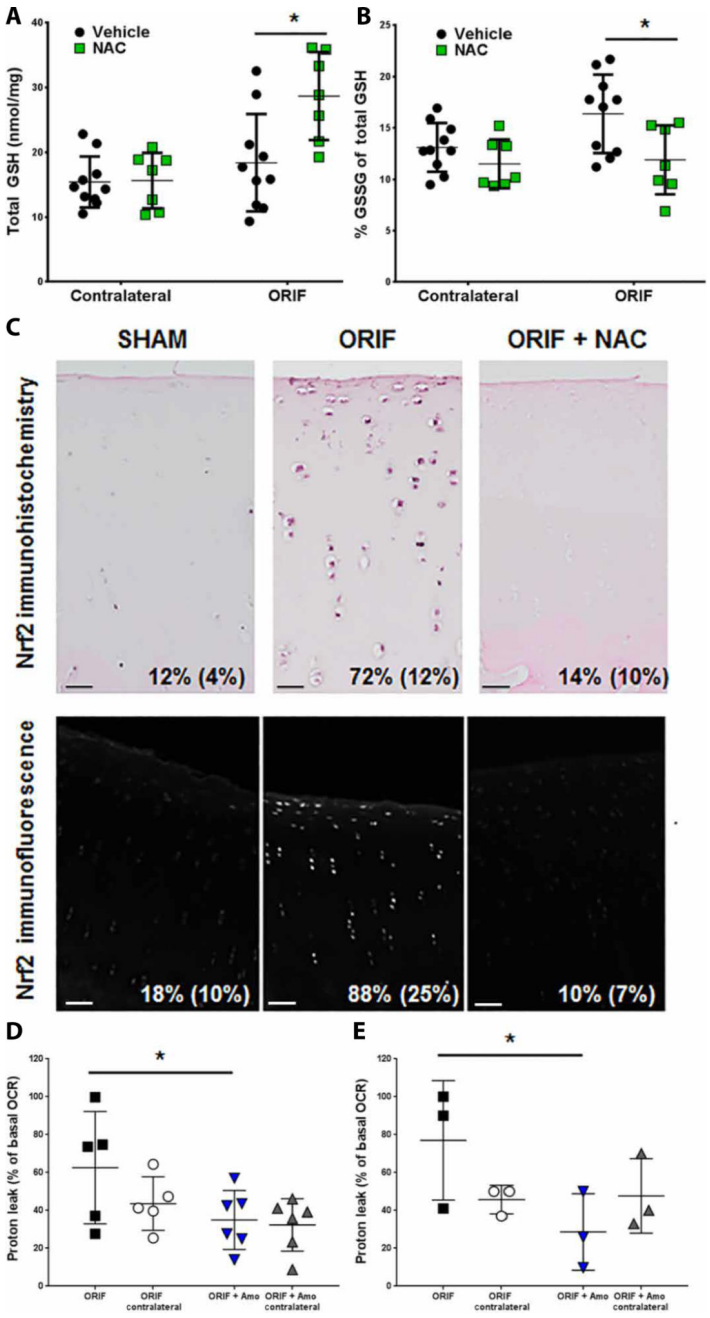

Fig. 4. NAC supplements intracellular GSH and prevents indications of oxidative stress after IAF

(**A**) Spectrophotometric analysis of total glutathione (GSH) concentrations of porcine articular cartilage, both tibial and talar with contralateral joints also shown, 1 week after IAF (n = 10 for ORIF + vehicle, n = 7 for ORIF + NAC; * $P < 0.01$ versus ORIF via Student's t-test). (**B**) Percent of total GSH present as oxidized glutathione disulfide (GSSG) 1 week after IAF (n = 10 for ORIF + vehicle, n = 7 for ORIF + NAC; * $P < 0.01$ versus ORIF via Student's t-test). (**C**) Representative images of immunohistochemical staining for Nrf2 1 week after IAF with percent positive cells per 20X field shown (n = 4 for both groups) in the top row and representative images of confocal immunofluorescent staining for Nrf2 1 week

after IAF with percent positive cells per 20X field shown (n = 4 for both groups) in the bottom row. Scale bars, 25 μm. Percentages indicate percent positive cells (SD). (**D**) Proton leak expressed as a percentage of basal oxygen consumption rate according to standard mitochondrial stress tests conducted on bovine chondrocytes 1 week after IAF (n = 10 for ORIF, n = 7 for ORIF + NAC; * $P < 0.05$). (**E**) Proton leak expressed as a percentage of basal oxygen consumption rate (OCR) conducted on freshly harvested rabbit chondrocytes 1 week after impact injury (n = 3 for both groups; * $P < 0.05$ via Student's t-test). Data represent the mean with SD shown.

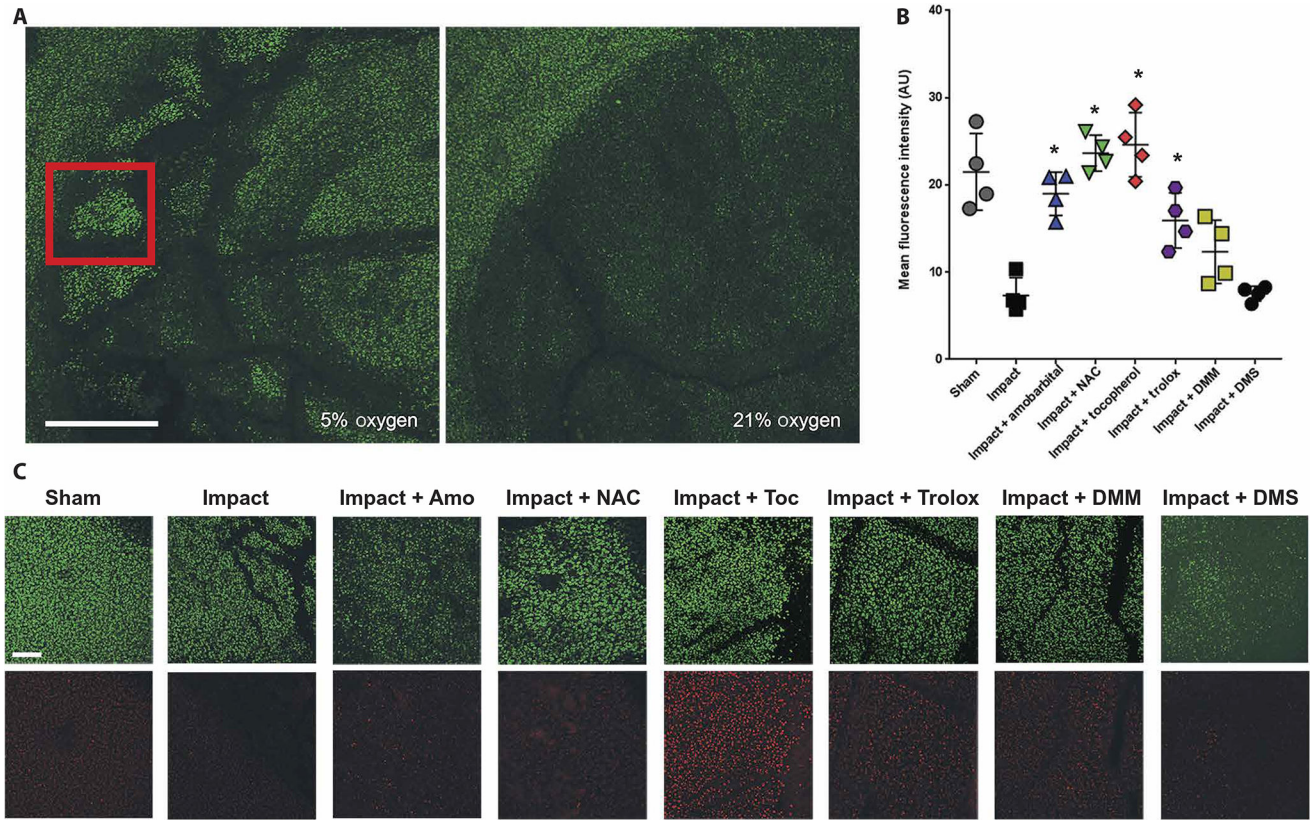

Fig. 5. Acute loss of mitochondrial content after impact is prevented by inhibition of electron transport or critical redox events

(**A**) Representative confocal micrographs at 4X magnification showing the site of a 2 J impact to bovine femoral osteochondral explants 24 hours after injury in either 5 or 21% oxygen. Scale bar, 1 mm. Red inset square indicates zone of interest for quantitation (**B**) and images shown in (**C**). (**B**) Quantitation of MitoTracker Deep Red staining 24 hours after 2 J impact (n = 4; * $P < 0.01$ versus impact alone via one-way ANOVA). Data represent the mean with SD shown. AU, arbitrary units. (**C**) Representative 10X micrographs of areas within the impact site as indicated by the red square in (**A**) and an analogous region central to the sham (unimpacted) osteochondral explant was chosen. Scale bar, 100 μm. Calcein AM is shown in green in the top row and MitoTracker Deep Red is shown in red in the bottom row. Amobarbital, NAC, α-tocopherol (Toc), trolox, dimethylmalonate (DMM), and dimethyl succinate (DMS) were all tested. Dark areas within the images indicate cracks or other structural damage from the impacts.

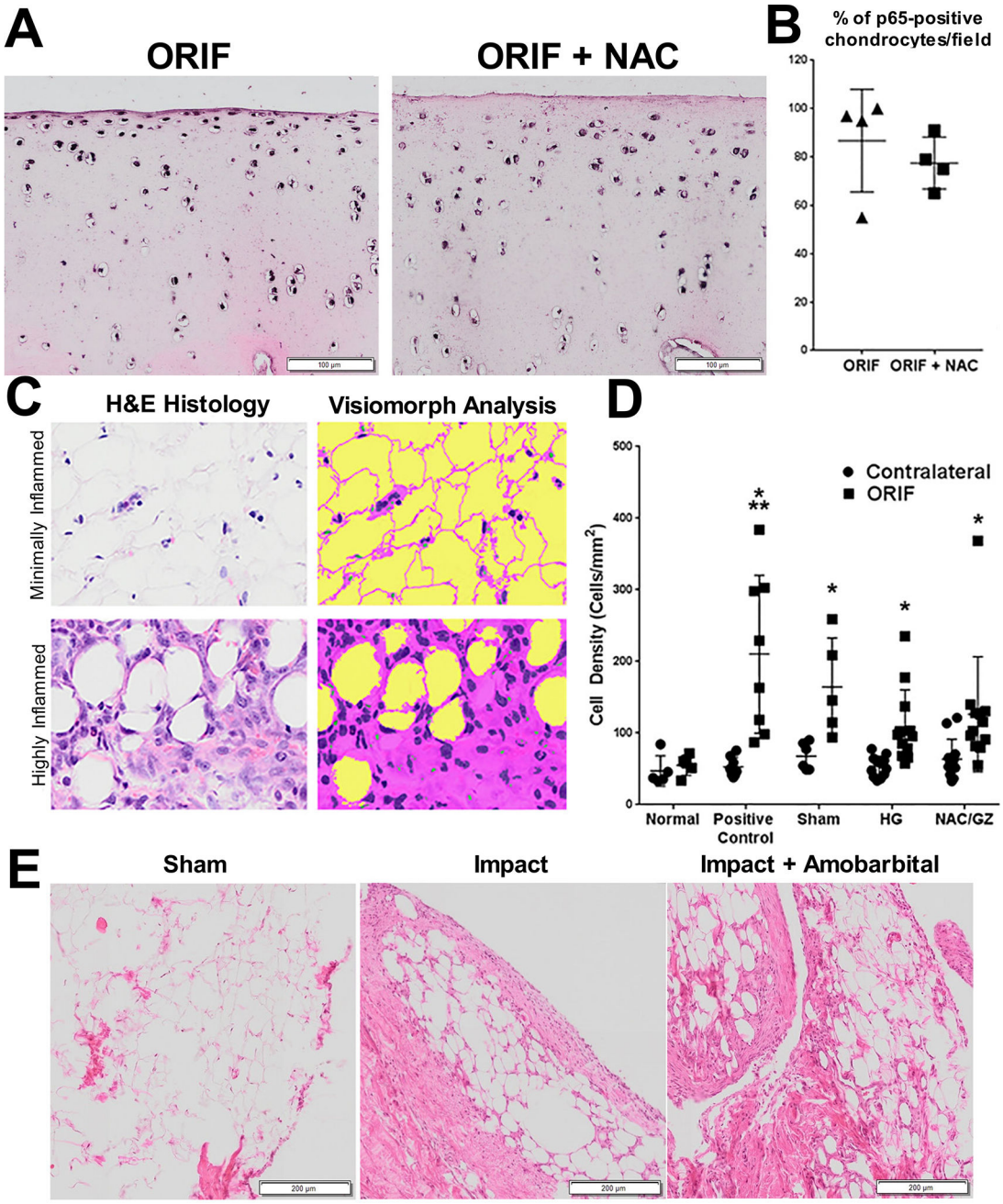

Fig. 6. Increases in joint inflammation 1 week after IAF were not prevented by NAC or amobarbital

(**A**) Representative micrographs from porcine anterior talar specimens 1 week after IAF with and without NAC (and glycyrrhizin, an agent intended to decrease inflammation that had a minimal, if any, effect and was added in this treatment group only) that have been formalin fixed and immunohistochemically stained for p65. (**B**) Quantitation of percent p65 positive-staining cells per 20X field from (**A**) (n = 4 for all groups; no significant differences noted via Student's t-test). (**C**) Illustration of the tissue and cell identification routine developed in Visiomorph software shown under minimally (top) and highly (bottom) inflamed conditions.

In the analysis of hematoxylin and eosin (H&E) images, tissue is classified as pink, cell nuclei as purple, and empty space as yellow. Cell counts and tissue areas are calculated from these color-coded images. (**D**) Average monocyte infiltration quantified from porcine infrapatellar fat pads 1 week after ORIF and a single treatment injection of either hydrogel only (HG) or NAC and glycyrrhizin (NAC/GZ) (n = 5 for normal, n = 8 for positive control, n = 6 for sham, n = 12 for HG and n = 12 for NAC/GZ; * $P < 0.01$ ORIF versus contralateral for each group except normal via two way ANOVA; ** $P < 0.01$ for positive control ORIF versus sham ORIF only). Data represent the mean with SD shown. (**E**) Representative micrographs of rabbit stifle (knee) synovia 1 week after severe impact stained with H&E (n = 3). Scale bar, 250 mm.

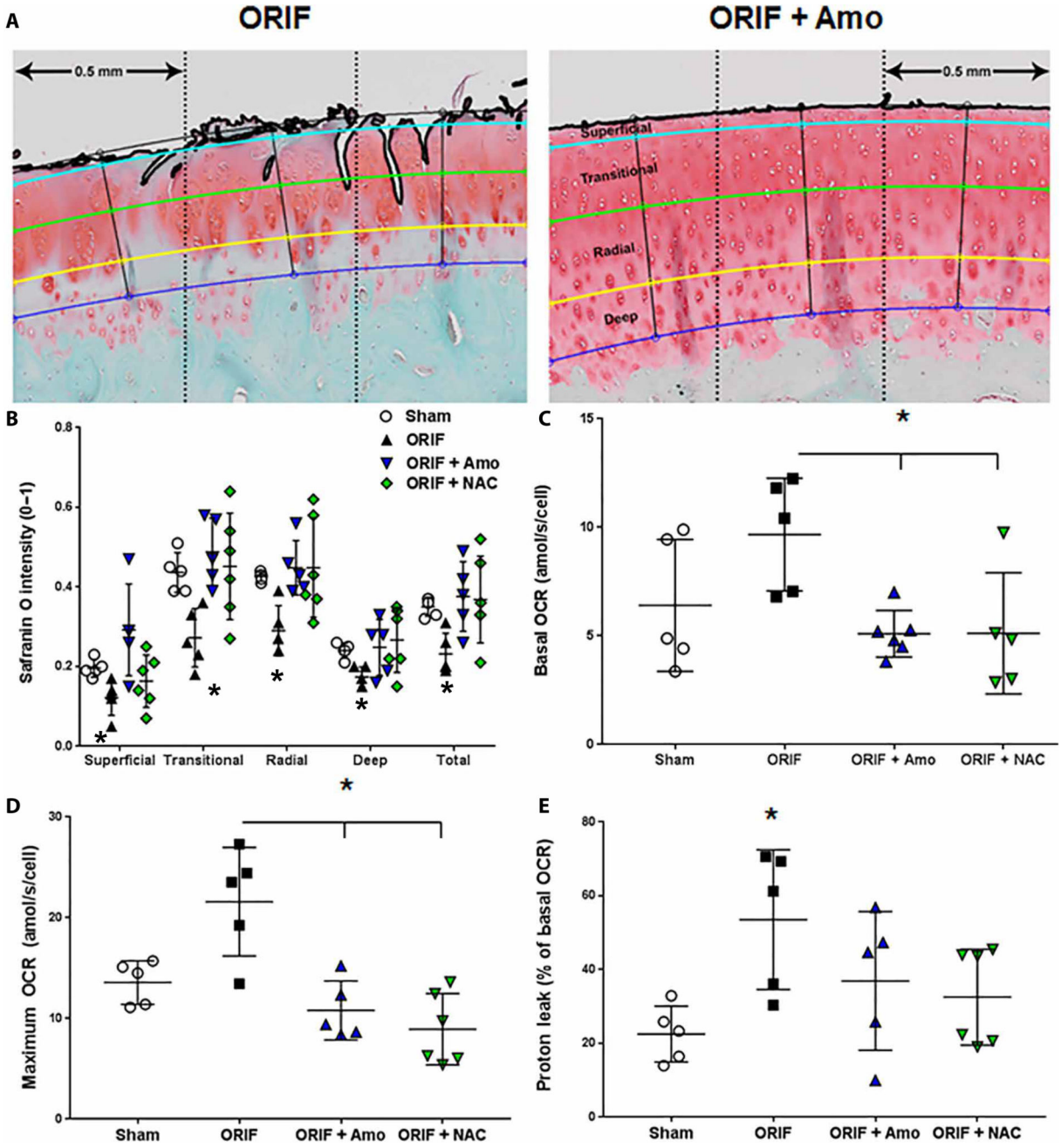

Fig. 7. Articular chondrocytes from amobarbital- and NAC-treated IAFs exhibit healthy anabolism 6 months after IAF

(**A**) Representative images of the semiautomated segmentation of porcine articular cartilage show how the scoring algorithm defines and tracks input from the different zones of the articular tissue in a continuum along the length of the entire specimen. (**B**) Local intensities of safranin O staining throughout the different zones of the porcine articular cartilage (* $P <$ 0.01 comparing the ORIF to other groups via two way ANOVA with Dunnett's posttest). (**C**) Basal OCRs of freshly harvested porcine chondrocytes 6 months after IAF (n = 5 for sham, n = 5 for ORIF, n = 5 for ORIF + amobarbital, n = 6 for ORIF + NAC; * $P <$ 0.01 versus ORIF via two way ANOVA with Dunnett's posttest). (**D**) OCRs after uncoupling (maximum

OCR) (n = 5 for sham, n = 5 for ORIF, n = 5 for ORIF + amobarbital, n = 6 for ORIF + NAC; * $P < 0.01$ versus ORIF via two way ANOVA with Dunnett's posttest). (**E**) Proton leak measured in freshly harvested porcine chondrocytes normalized to basal OCR, 6 months after IAF (n = 5 for sham, n = 5 for ORIF, n = 5 for ORIF + amobarbital, n = 6 for ORIF + NAC; * $P < 0.05$ ORIF versus sham via two way ANOVA with Dunnett's posttest but no other differences noted). Data represent the mean with SD shown.